BOUNDED RELATIVE ORBITS ABOUT ASTEROIDS FOR FORMATION FLYING AND APPLICATIONS

Nicola Baresi, Daniel J. Scheeres and Hanspeter Schaub

8th International Workshop on Satellite Constellations and Formation Flying

Delft, Nederland **June 8–10, 2015**

IWSCFF-2015

BOUNDED RELATIVE ORBITS ABOUT ASTEROIDS FOR FORMATION FLYING AND APPLICATIONS

Nicola Baresi[*], Daniel J. Scheeres[†], and Hanspeter Schaub[‡]

The relative motion about 4179 Toutatis is studied in order to investigate the feasibility of formation flying as an alternative concept for future asteroid exploration missions. In particular, the existence of quasi-frozen orbits about slowly rotating bodies [1] allows to compute families of periodic orbits in the body-fixed frame of the asteroid. Since these periodic orbits are of the *center*×*center* type, quasi-periodic invariant tori are numerically calculated via Koleman's surface of sections approach and used to initialize spacecraft formations about the central body. [2] Numerical simulations show that the resulting in-plane and out-of-plane relative trajectories remain bounded over long time spans; i.e., more than 30 days.

INTRODUCTION

In this thriving era for small bodies exploration, it may be interesting to study the relative motion of satellites flying in a formation about asteroids or comets. Such a concept is not novel and has already been proposed as a potential benefit for several asteroid mitigation strategies. For instance, Maddock and Vasile considered formations of solar concentrators to deflect hazardeous Nearh Earth Asteroids (NEA) by surface ablation. [3] Alternatively, Gong et al. proved the reliability of solar-sail formations in displaced orbits as effective and powerful gravity tractors. [4]

A common denominator in the literature, however, is that the gravitational attraction of the asteroid is usually neglected or oversimplified. Both Gong [4] and Vasile [5] approximate the gravitational pull excerted by the central body via a point-mass gravity field. Only recently, Foster et al. considered multiple gravity tractors in a high-order spherical harmonics gravity field, but instead of designing cost-free relative trajectories, the

[*]Graduate Research Assistant, Department of Aerospace Engineering Sciences, University of Colorado Boulder, 80309 Boulder, CO. mail: nicola.baresi@colorado.edu

[†]A. Richard Seebass Endowed Chair Professor, Department of Aerospace Engineering Sciences, University of Colorado Boulder, 80309 Boulder, CO. mail: scheeres@colorado.edu

[‡]Professor, Department of Aerospace Engineering Sciences, University of Colorado Boulder, 80309 Boulder, CO. mail: hanspeter.schaub@colorado.edu

authors were focused on controlling the satellites at fixed locations with respect to the Sun-asteroid rotating frame to maximize the effects of their proposed deflection strategy.[6] Accordingly, passive relative orbits in the proximity of small bodies are yet to be found and described.

In this paper, a systematic approach to establish bounded relative motion about slowly rotating tri-axial ellipsoids is presented. As a case study, a chief and a deputy spacecraft are considered while flying in a formation about 4179 Toutatis, a slowly rotating asteroid that was flown-by China's Chang'e 2 spacecraft in December 2012.[7] Because of the existence of quasi-frozen orbits in the body-fixed frame of the asteroid,[1] the secular evolution of the mean orbit elements of the satellites can be studied via Lagrange Planetary Equations.[10] Moreover, first-order bounded relative motion conditions can be derived by matching the averaged drift rates due to the nonspherical shape of the central body.[8] As these bounded relative motion conditions are based on mean orbit element differences, the applicability of using a first-order mean-to-osculating orbit element mapping for spacecraft formations about Toutatis is also investigated and used to motivate additional numerical analyses. Specifically, stable periodic orbits are computed starting from the output of the mean-to-osculating orbit element mapping and using a Poincaré map between consecutive surface of section crossings.[9] Then, Koleman's method is applied to extend the center manifolds beyond the linear regime, and to compute quasi-periodic orbits that foliate two dimensional invariant tori that surround the original periodic orbit.[2] Finally, the relative motion between satellites initialized on the quasi-periodic tori as well as on the computed periodic orbit is studied. In particular, numerical simulations investigate the long-term behaviour of the relative motion and assess the robustness of the derived initial conditions while taking into account unmodeled forces such as solar radiation pressure and third body attraction.

BOUNDED RELATIVE ORBIT CONDITIONS

According to Reference 9, the majority of the perturbations felt by mass particles about asteroids are due to the second degree and order gravity field. Thus, for preliminary Formation Flying mission analyses, it is possible to consider the gravitational potential as given by

$$U = \frac{\mu}{r}\left\{1 + \left(\frac{r_0}{r}\right)^2\left[C_{20}\left(\frac{3}{2}\sin^2\delta - \frac{1}{2}\right) - 3\,C_{22}\,\cos\left(2\,\lambda\right)\left(\sin^2\delta - 1\right)\right]\right\}, \quad (1)$$

where μ is the gravitational parameter of the central body, r is the distance of the satellite from the center of the asteroid, δ and λ are its latitude and longitude with respect to the first principal axis, r_0 is the scale factor, and $C_{20} = -J_2$ and C_{22} are respectively the second zonal and second-degree second-order spherical harmonics coefficients.

Furthermore, by definition

$$\sin\delta = \sin i\,\sin u, \tag{2a}$$

$$\tan\lambda = \frac{\sin\Omega_R\,\cos u + \cos\Omega_R\,\sin u\,\cos i}{\cos\Omega_R\,\cos u - \sin\Omega_R\,\sin u\,\cos i}, \tag{2b}$$

where i is the inclination of the spacecraft, $u = \omega + f$ is the argument of latitude, $\Omega_R = \Omega - \omega_T\,t$ is the longitude of the ascending node with respect to the rotating body-fixed frame of the asteroid, and ω_T is the spin rate of the central body. Therefore, it is possible to consider the averaged perturbing function

$$\bar{R} = \frac{\mu\,r_0^2}{2\,a^3\,(1-e^2)^{3/2}}\left[C_{20}\left(\frac{3}{2}\,\sin^2 i - 1\right) - 3\,C_{22}\,\sin^2 i\,\cos\left(2\,\Omega_R\right)\right] \tag{3}$$

and investigate the evolution of the spacecraft mean orbit elements with Lagrange Planetary Equations.[10]

It turns out that for a very slow rotator such as 4179 Toutatis ($P_T = 2\,\pi/\omega_T \simeq 5.43$ days) the mean orbital element rates can be rewritten as[1;8]

$$a' = 0, \tag{4a}$$

$$e' = 0, \tag{4b}$$

$$i' = \frac{3\,C_{22}\,\sin i\,\sin\left(2\,\Omega_R\right)}{\eta^4 L^7}, \tag{4c}$$

$$\Omega_R' = \frac{3\,\cos i\,(C_{20} + 2\,C_{22}\,\cos\left(2\,\Omega_R\right))}{2\,\eta^4\,L^7} - \frac{\omega_T}{n_0}, \tag{4d}$$

$$\omega' = -\frac{15\,\cos\left(2i\right)\,(C_{20} + 2\,C_{22}\,\cos\left(2\,\Omega_R\right)) + 9\,C_{20} - 6\,C_{22}\,\cos\left(2\,\Omega_R\right)}{8\,\eta^4\,L^7}, \tag{4e}$$

$$M' = \frac{1}{L^3} + \frac{9\,\sin^2 i\,(C_{20} + 2\,C_{22}\,\cos\left(2\,\Omega_R\right)) - 6\,C_{20}}{4\,\eta^3\,L^7}, \tag{4f}$$

where

$$(\cdot)' = \frac{1}{n_0}\,\frac{\mathrm{d}}{\mathrm{d}\,t}, \tag{5a}$$

$$n_0 = \sqrt{\mu/r_0^3}, \tag{5b}$$

$$\eta = \sqrt{1-e^2}, \tag{5c}$$

$$L = \sqrt{a/r_0}. \tag{5d}$$

Accordingly, the semi-major axis and the eccentricity are constant on average, whereas the inclination, body-fixed longitude of ascending node, argument of periapse, and mean

anomaly vary with time depending on a, e, i, and Ω_R. This may become an issue as the (4) are derived assuming that the orbit elements of the spacecraft can be regarded as constant over one orbital period. For motion about small bodies, this is hardly true unless $P << P_T$, where P is the orbital period of the spacecraft and $P_T = 2\,\pi/\omega_T$. In this case, both the mean inclination and body-fixed longitude of the ascending node rates can be nulliefied by imposing the quasi-frozen orbit conditions derived by Hu and Scheeres:[1]

$$\Omega_R = \pm\pi/2, \tag{6a}$$

$$\cos i = -\omega_T/B, \tag{6b}$$

where

$$B = \frac{3\,n}{2\,p^2}\,\left[2\,C_{22} - C_{20}\right]\,r_0^2. \tag{7}$$

Then, Eq. (4) becomes a reliable set of equations that can be used to infer second-order second-degree bounded relative motion conditions.

From now on, a, e, i, Ω_R, ω, and M will be referred to as the mean orbit elements of the chief spacecraft, whereas a_d, e_d, i_d, $\Omega_{R,d}$, ω_d, and M_d will be used to indicate the mean orbit elements of the deputy. We will also refer to $\delta i'$, $\delta\Omega'_R$, $\delta\omega'$, and $\delta M'$ as the first variations of $i'_d - i'$, $\Omega'_{R,d} - \Omega'_R$, $\omega'_d - \omega'$, and $M'_d - M'$ respectively.

It can immediately be noted that $\delta i'$, $\delta\Omega'_R$, $\delta\omega'$, and $\delta M'$ would vanish if $L_d = L$, $\eta_d = \eta$, $i_d = i$, and $\Omega_{R,d} = \Omega_R$ (in-plane formations). Such a selection would guarantee bounded relative motion but would not leave much freedom in the design of the relative trajectory. The same happen whenever the chief and the deputy are initialized with the same set of mean orbit elements, except for the mean anomaly at epoch, i.e., $M_d \neq M$ (Leader-Follower formations). Alternatively, following the derivation of the J_2-invariant relationships,[8] one could look at the first variation of the mean argument of latitude, i.e., $\theta_M = M + \omega$, and try to nullify $\delta\theta'_M = \delta M' + \delta\omega'$ instead of (4e) and (4f). Thus, the more general second-order second-degree bounded relative orbit relationships would be given by

$$\delta i' = \frac{\partial i'}{\partial L}\,\delta L + \frac{\partial i'}{\partial \eta}\,\delta\eta + \frac{\partial i'}{\partial i}\,\delta i + \frac{\partial i'}{\partial \Omega_R}\,\delta\Omega_R = 0, \tag{8a}$$

$$\delta\Omega'_R = \frac{\partial \Omega'_R}{\partial L}\,\delta L + \frac{\partial \Omega'_R}{\partial \eta}\,\delta\eta + \frac{\partial \Omega'_R}{\partial i}\,\delta i + \frac{\partial \Omega'_R}{\partial \Omega_R}\,\delta\Omega_R = 0, \tag{8b}$$

$$\delta\theta'_M = \frac{\partial \theta'_M}{\partial L}\,\delta L + \frac{\partial \theta'_M}{\partial \eta}\,\delta\eta + \frac{\partial \theta'_M}{\partial i}\,\delta i + \frac{\partial \theta'_M}{\partial \Omega_R}\,\delta\Omega_R = 0. \tag{8c}$$

From Equations (8a) and (8b), it follows that

$$C_{22}\,\sin\left(2\,\Omega_R\right)\,\left[\eta\,L\,\cos i\,\delta i-\sin i\,\left(4\,L\,\delta\eta+7\,\eta\,\delta L\right)\right]$$
$$+2\,C_{22}\,\eta\,L\,\sin i\,\cos\left(2\,\Omega_R\right)\,\delta\Omega_R=0, \tag{9a}$$
$$\left[C_{20}+2\,C_{22}\,\cos\left(2\,\Omega_R\right)\right]\,\left[\cos i\,\left(4\,L\,\delta\eta+7\,\eta\,\delta L\right)+\delta i\eta\,L\,\sin i\right]$$
$$+4\,C_{22}\,\eta\,L\,\cos i\,\sin\left(2\,\Omega_R\right)\,\delta\Omega_R=0, \tag{9b}$$

which, when evaluated at the quasi-frozen orbit conditions (6a)-(6b), simplify in

$$-\frac{2}{B}\,C_{22}\,\omega_T\,\eta\,L\,\Gamma\,\delta\Omega_R=0, \tag{10a}$$
$$-7\,\eta\,\delta L-4\,L\,\delta\eta+\eta\,L\,\Gamma\,\delta i=0, \tag{10b}$$

with

$$\Gamma=\sqrt{\left(B/\omega_T\right)^2-1}. \tag{11}$$

Consequently, in order to satisfy the bounded relative orbit conditions (8a)–(8c), $\delta\Omega_R$ must always be equal to zero, i.e., $\Omega_{R,d}=\Omega_R$. Furthermore, substituting Eq. (10a) and (10b) into Eq. (8c) yields

$$\delta i=\frac{B^2\,\left(7\,C_{20}-42\,C_{22}+16\,\eta^3\,L^4\right)-21\,\omega_T^2\,\left(C_{20}-2\,C_{22}\right)}{B^2\,\left[7\,\left(\eta+1\right)\,\left(C_{20}-6\,C_{22}\right)+4\,\eta^4\,L^4\right]+7\,\omega_T^2\,\left(3\,\eta+5\right)\,\left(C_{20}-2\,C_{22}\right)}\,\frac{1}{\Gamma}\,\delta\eta, \tag{12}$$

which can also be substituted back into Eq. (10b) to get the final set of first-order mean orbit element relationships as a function of $\delta\eta$:

$$\delta L=-\frac{\left(3\,\eta+4\right)\,L\,\left[B^2\,\left(C_{20}-6\,C_{22}\right)+5\,\omega_T^2\,\left(C_{20}-2\,C_{22}\right)\right]}{B^2\,\left[7\,\left(\eta+1\right)\,\left(C_{20}-6\,C_{22}\right)+4\,\eta^4\,L^4\right]+7\,\omega_T^2\,\left(3\,\eta+5\right)\,\left(C_{20}-2\,C_{22}\right)}\,\frac{1}{\eta}\,\delta\eta. \tag{13}$$

Thus, for any reasonable value of $\delta\eta=\eta_d-\eta$, the Equations (12) and (13) give the mean inclination and semi-major axis differences that minimize the secular drift induced by second-order second-degree gravity terms. Also notice that for $C_{22}=0$, $\omega_T=-B\,\cos i$, the Eq. (12) and (13) reduce to the full J_2-invariant orbit relationships derived in Reference 8.

MEAN/OSCULATING ORBIT ELEMENT MAPPINGS

The second-order second-degree bounded relative orbit conditions have been derived in the mean orbit element space. Thus, it is necessary to implement a reliable mean-to-osculating orbit element mapping in order to design spacecraft formation about slowly rotating asteroids. To that end, a first-order Lie-Deprit transformation is implemented to convert from mean to osculating orbit elements and vice versa.[11] The generating functions used for the conversion can be found in De Saedeleer and Henrard.[12]

Figure 1 shows a comparison between two different chief trajectories integrated in the rotating body-fixed frame of the asteroid for four weeks, i.e., more than 70 Orbital Periods (OP), with a second-order second-degree gravity field.[9] Both the trajectories are initialized on a quasi-frozen orbit with keplerian orbit elements given by

$$\begin{aligned} \mathfrak{oe}_c &= \begin{bmatrix} a & e & i & \Omega & \omega & M \end{bmatrix}^T, \\ &= \begin{bmatrix} 3800 & 0.10 & 147.22 & 90.00 & 0.00 & 180.00 \end{bmatrix}^T \qquad \text{(m, -, deg).} \end{aligned} \tag{14}$$

However, in the plot on the right the initial conditions (14) are first converted with the aforementioned Lie-Deprit transformation.

As expected, the mean orbit element initialized trajectory displays a much more stable behaviour than the one initialized in the osculating orbit element space. However, the time histories of the chief osculating orbit elements shown in Figure 2 reveal that second-order effects can hardly be neglected for orbiters about Toutatis ($C_{20} \simeq -0.31$,

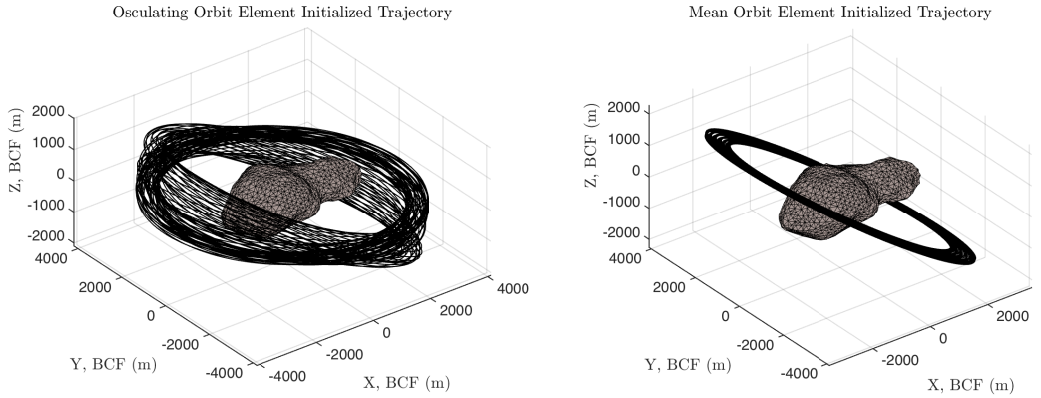

Figure 1: Osculating and Mean Orbit Element Initialized Chief Trajectories.

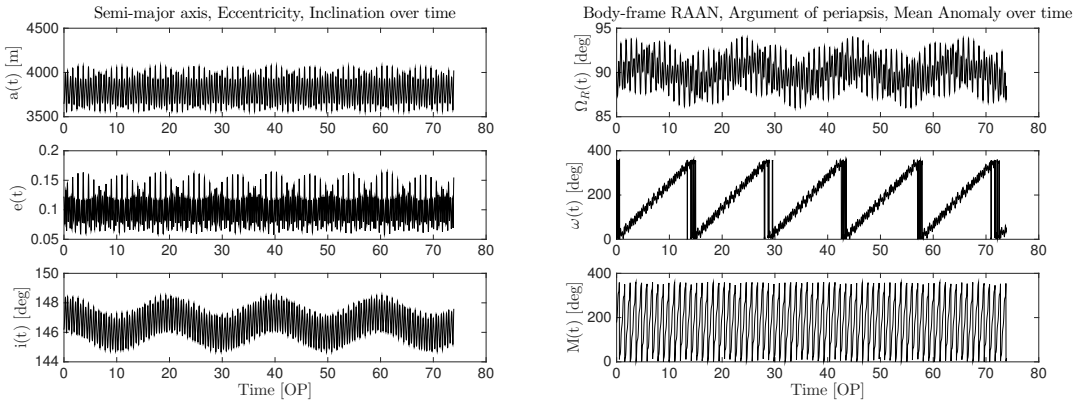

Figure 2: Osculating orbit elements for the mean orbit element initialized trajectory.

$C_{22} \simeq 0.12$). This is even more evident when we compare different relative trajectories computed with the same mean-to-osculating orbit element mapping but using different initial conditions for the chief (Figures 3–5). Even though the relative trajectories are more performant than the standard J_2 invariant orbits, their stability seems to vary with the initial conditions of the chief spacecraft. Therefore, the first-order Lie-Deprit transformation currently available in the literature does not seem to be accurate enough to design long-term relative trajectories about strongly elongated bodies. Instead, consider the strategy outlined in the next sections, which involves the computation of periodic and quasi-periodic orbits about Toutatis.

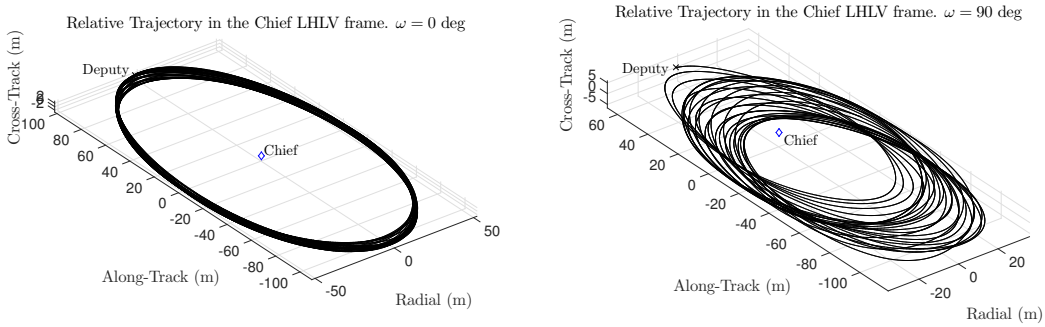

Figure 3: In-plane relative trajectories with $\delta\omega = -\delta M = 8$ deg, and $\omega = 0$ and 90 deg respectively.

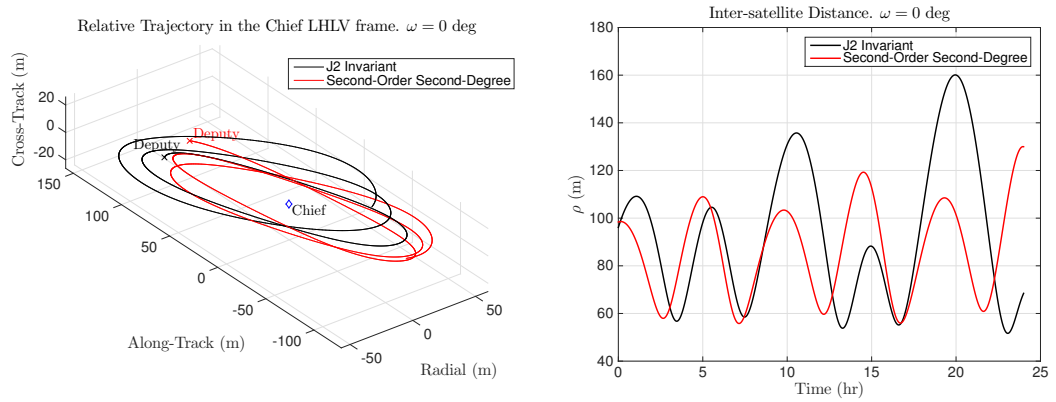

Figure 4: J_2-invariant and second-order second-degree out-of-plane relative trajectories with $\delta i = 0.4$ deg, $\delta\omega = 8$ deg, $\delta M = -8$ deg, and $\omega = 0$ deg.

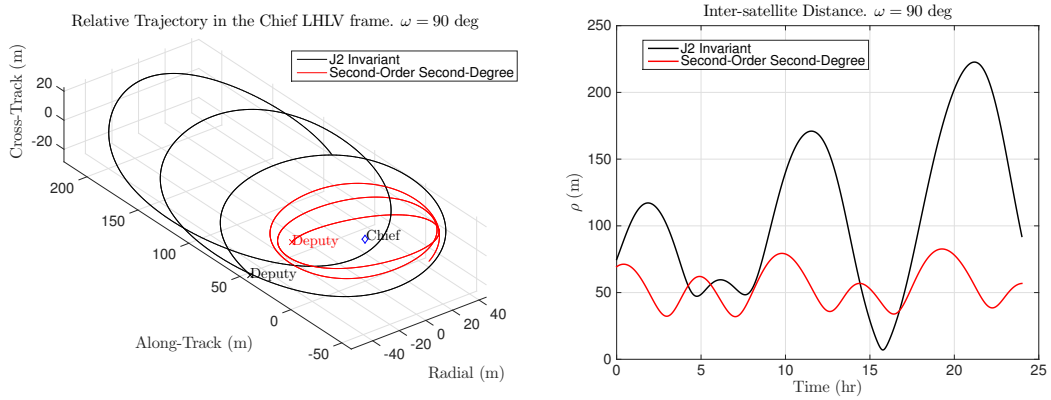

Figure 5: J_2-invariant and second-order second-degree out-of-plane relative trajectories with $\delta i = 0.4$ deg, $\delta\omega = 8$ deg, $\delta M = -8$ deg, and $\omega = 90$ deg.

EQUATIONS OF MOTION

In order to compute periodic orbits, consider the equations of motion for one spacecraft in orbit about 4179 Toutatis. The asteroid is modeled as a tri-axial ellipsoid with semi-major axes $\alpha = 2250$ m, $\beta = 1200$ m, and $\gamma = 950$ m (Figure 6). Moreover, although Toutatis is a non-principal axis rotator,[13] it is assumed that the angular velocity vector of the body is aligned with the third axis $\hat{\boldsymbol{e}}_3$ of an inertial reference frame $\mathcal{N} = \{\mathcal{O}, \hat{\boldsymbol{e}}_1, \hat{\boldsymbol{e}}_2, \hat{\boldsymbol{e}}_3\}$ centered on the body and oriented such that $\hat{\boldsymbol{e}}_1$, $\hat{\boldsymbol{e}}_2$, and $\hat{\boldsymbol{e}}_3$ are parallel to the asteroid principal axes of inertia at time $t_0 = 0$. Then, a second rotating reference frame can be defined such that $\hat{\boldsymbol{b}}_1$, $\hat{\boldsymbol{b}}_2$, and $\hat{\boldsymbol{b}}_3$ are always aligned with the asteroid principal axes of inertia. Thus, let $\mathcal{B} = \{\mathcal{O}, \hat{\boldsymbol{b}}_1, \hat{\boldsymbol{b}}_2, \hat{\boldsymbol{b}}_3\}$ be denoted as the Body-Centered-Body-Fixed frame (BCF) and $\mathcal{N} = \{\mathcal{O}, \hat{\boldsymbol{e}}_1, \hat{\boldsymbol{e}}_2, \hat{\boldsymbol{e}}_3\}$ as the Body-Centered-Inertial frame (BCI), with $\boldsymbol{\omega}_{\mathcal{B}/\mathcal{N}} = \omega_T \hat{\boldsymbol{b}}_3$, $\omega_T = 1.34 \times 10^{-5}$ rad/s as the angular velocity of the $\mathcal{B}$ frame as seen by the inertial frame $\mathcal{N}$.

In BCF, the equations of motion of a single satellite are given by

$$\begin{cases} \ddot{x} &= \omega_T^2\, x + 2\,\omega_T\, \dot{y} + U_x + f_x, \\ \ddot{y} &= \omega_T^2\, y - 2\,\omega_T\, \dot{x} + U_y + f_y, \\ \ddot{z} &= U_z + f_z, \end{cases} \tag{15}$$

where $\boldsymbol{r} = x\,\hat{\boldsymbol{b}}_1 + y\,\hat{\boldsymbol{b}}_2 + z\,\hat{\boldsymbol{b}}_3$ is the position vector of the satellite, U_x, U_y, U_z are the $\mathcal{B}$-frame components of the gravitational acceleration exerted by the central body, and f_x, f_y, f_z are the $\mathcal{B}$-frame components of control input vectors and/or external perturbations acting on the system (e.g., solar radiation pressure and third body attraction).

Following Reference 14, the body-fixed coordinates of the gravitational attraction excerted by a constant density tri-axial ellipsoid can be computed analytically from the

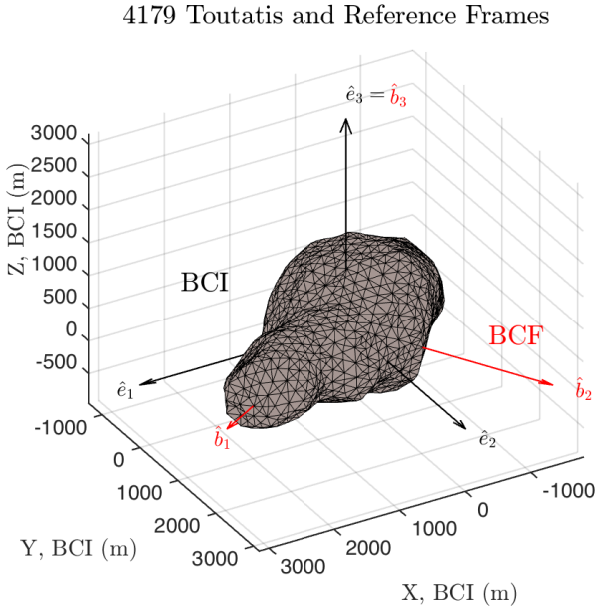

Figure 6: Asteroid 4179 Toutatis and Reference Frames.

partial derivatives of the potential

$$U = -\mu \frac{3}{4} \int_0^\infty \phi(x, y, z, v + \Lambda) \frac{dv}{\Delta(v + \Lambda)}, \tag{16}$$

where

$$\Delta(v + \Lambda) = \sqrt{(\alpha^2 + \Lambda + v)(\beta^2 + \Lambda + v)(\gamma^2 + \Lambda + v)}, \tag{17a}$$

$$\phi(x, y, z, v + \Lambda) = \frac{x^2}{\alpha^2 + \Lambda + v} + \frac{y^2}{\beta^2 + \Lambda + v} + \frac{z^2}{\gamma^2 + \Lambda + v} - 1. \tag{17b}$$

Observe that U depends on both the gravitational parameter of the body, i.e.,

$$\mu = 1792.60 \text{ m}^3/\text{s}^2, \tag{18}$$

and Λ, which is defined to be either the positive root of $\phi(x, y, z, \Lambda) = 0$ whenever U is computed outside of the ellipsoid, or zero otherwise.

It is also worth noting that the system (15) admits an integral of motion given by

$$C = -\frac{1}{2}(\dot{x}^2 + \dot{y}^2 + \dot{z}^2) + \frac{1}{2}\omega_T^2 (x^2 + y^2) + U, \tag{19}$$

which is also known as the Jacobi integral. Furthermore, it turns out that the equations of motion (15) can be easily linearized via

$$\dot{\boldsymbol{X}} = \big[A\big]\, \boldsymbol{X} \tag{20}$$

where $\boldsymbol{X} = \begin{bmatrix} x & y & z & \dot{x} & \dot{y} & \dot{z} \end{bmatrix}^T$,

$$[A] = \begin{bmatrix} 0 & 0 & 0 & 1 & 0 & 0 \\ 0 & 0 & 0 & 0 & 1 & 0 \\ 0 & 0 & 0 & 0 & 0 & 1 \\ \omega_T^2 + U_{xx} & U_{xy} & U_{xz} & 0 & 2\,\omega_T & 0 \\ U_{xy} & \omega_T^2 + U_{yy} & U_{yz} & -2\,\omega_T & 0 & 0 \\ U_{xz} & U_{yz} & U_{zz} & 0 & 0 & 0 \end{bmatrix}, \tag{21}$$

and U_{xx}, U_{xy}, U_{xz}, U_{yy}, U_{yz}, and U_{zz} are the second partial derivatives of the potential (16). Accordingly, the State Transition Matrix $\Phi(t, t_0)$ can also be integrated along with Eq. (15) via

$$\dot{\Phi}(t, t_0) = [A]\,\Phi(t, t_0), \qquad \Phi(t_0, t_0) = [I_{6\times 6}], \tag{22}$$

where $I_{6\times 6}$ is the 6×6 identity matrix.

PERIODIC ORBITS ABOUT 4179 TOUTATIS

Integrating the initial conditions provided by the Lie-Deprit transformation with Eq. (15) yields the trajectory portrayed in Figure 7a. As it can be seen, the satellite is very close to be on a periodic trajectory, and further numerical investigation can be carried on to achieve periodic motion.

To that end, notice that the spacecraft passes through the x-y plane twice along its orbit: one with $\dot{z} > 0$, and one with $\dot{z} < 0$. Accordingly, $S(\boldsymbol{x}) = z$, $\dot{z} < 0$ is a valid surface of section that can be used to compute a linearized Poincaré Map and its associated monodromy matrix.[9]

Given the reduced state $\boldsymbol{y} = \begin{bmatrix} x & y & \dot{x} & \dot{y} \end{bmatrix}^T$, it turns out that deviations on the surface of section at time t_0, namely $\delta\boldsymbol{y}_0$, can be mapped into deviations at the next surface of section crossing via

$$\begin{aligned} \delta\boldsymbol{y}_1 &= \Phi_{10}\,\delta\boldsymbol{y}_0, \\ &= P_0^T\,P_S\,\Phi(t_1, t_0)\,(P_0 + P_H)\,\delta\boldsymbol{y}_0 \end{aligned} \tag{23}$$

where

$$P_0 = \begin{bmatrix} I_{2\times 2} & 0_{2\times 2} \\ 0_{1\times 2} & 0_{1\times 2} \\ 0_{2\times 2} & I_{2\times 2} \\ 0_{1\times 2} & 0_{1\times 2} \end{bmatrix}, \qquad P_S = [I_{6\times 6}] - \frac{1}{\left.\dfrac{\partial S}{\partial \boldsymbol{x}}\right|_1 \cdot \dot{\boldsymbol{x}}(t_1)}\,\dot{\boldsymbol{x}}(t_1)\,\left.\frac{\partial S}{\partial \boldsymbol{x}}\right|_1, \tag{24}$$

$$P_H = \frac{1}{\dot{z}_0}\begin{bmatrix} 0 & 0 & 0 & 0 \\ 0 & 0 & 0 & 0 \\ 0 & 0 & 0 & 0 \\ 0 & 0 & 0 & 0 \\ 0 & 0 & 0 & 0 \\ (\omega_T^2\, x_0 + U_{x_0}) & (\omega_T^2\, y_0 + U_{y_0}) & -\dot{x}_0 & -\dot{y}_0 \end{bmatrix}. \tag{25}$$

Accordingly, if $\boldsymbol{y}_1 = \boldsymbol{g}(\boldsymbol{y}_0, C)$ is the full nonlinear Poincaré Map from an initial point $\boldsymbol{y}_0$ and fixed energy C to the next surface of section crossing $\boldsymbol{y}_1$,

$$\begin{aligned} \boldsymbol{y}_0 + \delta\boldsymbol{y}_0 &= \boldsymbol{g}(\boldsymbol{y}_0 + \delta\boldsymbol{y}_0, C), \\ &= \boldsymbol{g}(\boldsymbol{y}_0, C) + \left[\frac{\partial \boldsymbol{g}}{\partial \boldsymbol{y}}\right] \delta\boldsymbol{y}_0 + \ldots \\ &= \boldsymbol{y}_1 + [\Phi_{10}]\, \delta\boldsymbol{y}_0 + \ldots \end{aligned} \tag{26}$$

and

$$\delta\boldsymbol{y}_0 = [I_{4\times 4} - \Phi_{10}]^{-1}\, (\boldsymbol{y}_1 - \boldsymbol{y}_0). \tag{27}$$

The Equation (27) can be used to update the initial guess $\boldsymbol{y}_0$ until a fixed point for the linearized map is found. After five iteration, the algorithm converges to

$$\boldsymbol{y}_0 = \begin{bmatrix} 1.3185 \times 10^{-11} & 3679.9296 & 0.5812 & 2.1991 \times 10^{-14} \end{bmatrix}^T \quad \text{(m, m/s)} \tag{28}$$

which corresponds to the periodic orbit illustrated in Figures 7b ($C = 0.2145$, hence $\dot{z} = -0.4302$ m/s).

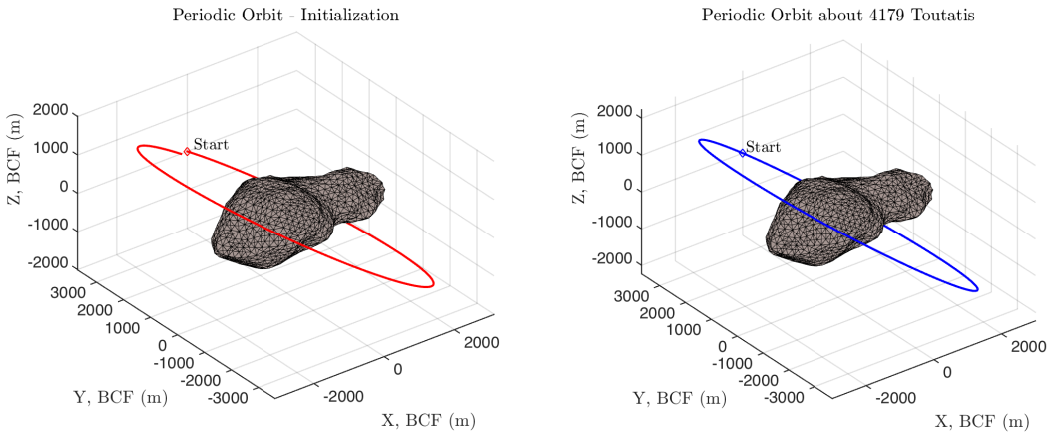

(a) (b)

Figure 7: Initial Guess and final Periodic Orbit in the BCF frame.

It is now possible to explore the continuation of the periodic orbit by varying the value of the Jacobi integral as follows: Given the periodic orbit of Figure 7b, $\boldsymbol{y}^* = \boldsymbol{g}(\boldsymbol{y}^*, C)$, therefore

$$\begin{aligned} \boldsymbol{y}^* + \delta\boldsymbol{y} &= \boldsymbol{g}(\boldsymbol{y}^* + \delta\boldsymbol{y}, C + \delta C), \\ &\simeq \boldsymbol{g}(\boldsymbol{y}^*, C) + \Phi_{10}\,\delta\boldsymbol{y} + \left[\frac{\partial \boldsymbol{g}}{\partial C}\right] \delta C, \end{aligned} \tag{29}$$

and

$$\delta\boldsymbol{y} = [I_{4\times 4} - \Phi_{10}]^{-1} \left[\frac{\partial \boldsymbol{g}}{\partial C}\right] \delta C, \tag{30}$$

where

$$\left[\frac{\partial \boldsymbol{g}}{\partial C}\right] = P_0^T\, P_S\, \Phi(T, 0) \begin{bmatrix} 0 & 0 & 0 & 0 & 0 & \dfrac{1}{C_{\dot{z}}} \end{bmatrix}^T, \tag{31a}$$

$$C_{\dot{z}} = \frac{\partial C}{\partial \dot{z}} = -\dot{z}. \tag{31b}$$

The new initial guess computed with (30) can now be used to initialize Eq. (27) and converge to a new periodic orbit at the value of energy $C = C^* + \delta C$. Figure 8 displays a family of periodic orbits computed at different values of the Jacobi constant for either $\Omega_R = -90$ deg or $\Omega_R = 90$ deg. As it can be seen, changing the value of C yields periodic orbits at different inclinations, thus giving the possibility to investigate the central body at different latitudes.

Also notice that the monodromy matrix $M = \Phi_{10}(T, 0)$ computed along the periodic orbits typically admit two pairs of complex conjugate eigenvalues with unity magnitude.

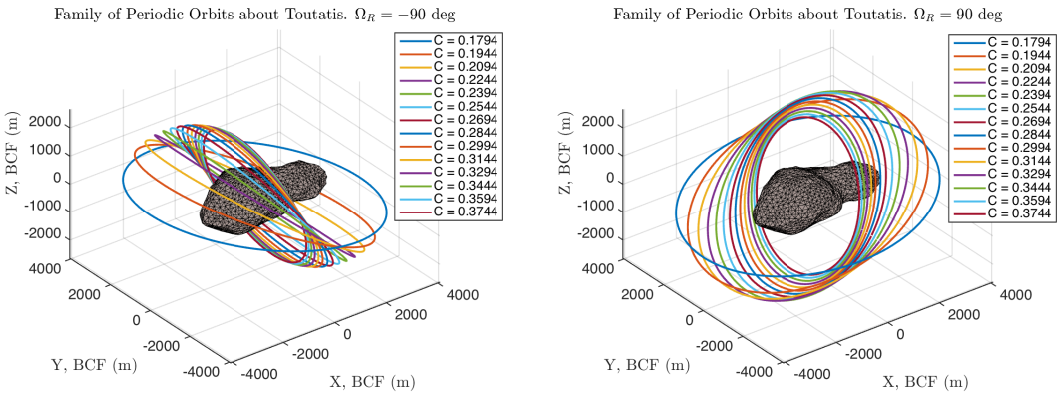

(a) (b)

Figure 8: Families of periodic orbits for $\Omega_R = -90$ deg and $\Omega_R = 90$ deg.

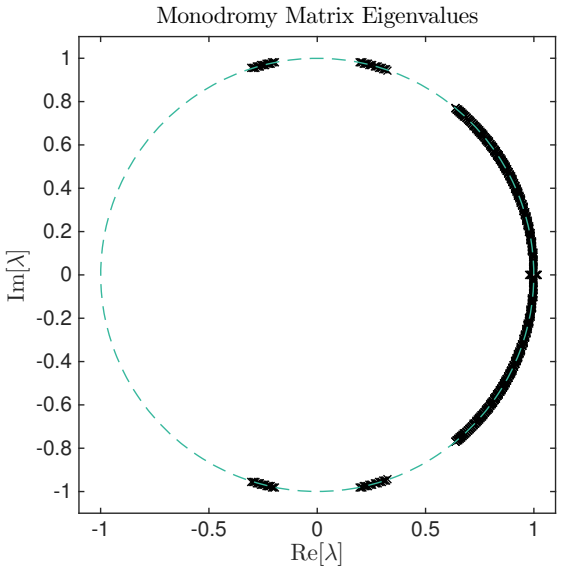

Figure 9: Distribution of the Monodromy matrix eigenvalues for families of periodic orbits about 4179 Toutatis.

That is, Figure 9 shows the root locus of M for the family of periodic orbits of Figure 8a. Except for a very few cases where the periodic orbit becomes unstable, the eigenvalues are usually distributed along the unit circle of the complex plane. In particular, for the periodic orbit of Figure 7b, the eigenvalues of the monodromy matrix are

$$\lambda_{12} = 0.9609 \pm \mathrm{i}\, 0.2770, \tag{32a}$$

$$\lambda_{34} = 0.9016 \pm \mathrm{i}\, 0.4326. \tag{32b}$$

Therefore, the periodic orbit turns out to be stable and surrounded by two center manifolds. Because of these center manifolds, initial conditions for long-term bounded relative motion about 4179 Toutatis can be found.

QUASI-PERIODIC ORBITS ABOUT TOUTATIS

By definition, center manifolds about periodic orbits are made by invariant tori that surround the periodic orbit itself.[9] If a spacecraft is initialized on the surface of a quasi-periodic torus, it will stay on it forever. Therefore, quasi-periodic invariant tori are natural candidates for computing initial conditions that yield bounded relative motion about slowly rotating asteroids.

Following the approach of Koleman et al.,[2] quasi-periodic tori can be computed as follows. First, notice that for a given eigenvalue/eigenvector pair, e.g., $\lambda = \lambda_{12}$, $\boldsymbol{v} = \boldsymbol{v}_{12} = \boldsymbol{v}_1 + \mathrm{i}\, \boldsymbol{v}_2$, it is possible to compute the invariant circle of the monodromy map

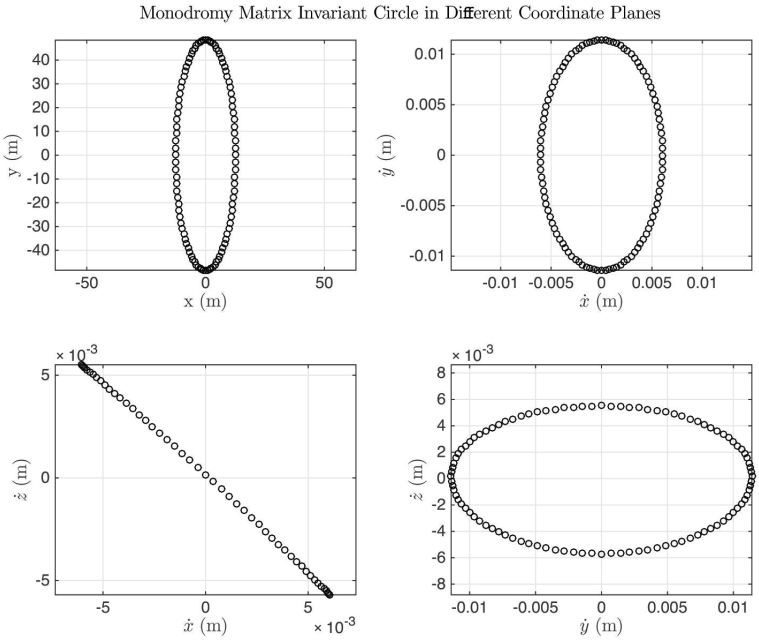

Figure 10: Monodromy Matrix Invariant Circle in Different Coordinate Planes.

M. That is, for any $\theta \in [0, 2\,\pi]$ and magnitude κ, we can define

$$\psi(\theta) = \kappa\, \cos\theta\, \boldsymbol{v}_1 - \kappa\, \sin\theta\, \boldsymbol{v}_2, \tag{33}$$

such that $M\,\psi(\theta) = \psi(\theta + \eta)$. Therefore, $\psi(\theta)$ is a periodic orbit of the map M (see Koleman's paper for proof).

Although $\psi(\theta)$ should not be confused with the invariant set of the Poincaré section defined by the intersection between the quasi-periodic torus and $S(\boldsymbol{x})$, it is a linear approximation of the relative distance between the torus and the periodic orbit under investigation. Therefore, it can be used to initialize a Newton iteration scheme aimed to compute the actual invariant set of the surface of section.

That is, consider $N = 100$ points on the invariant circle of the map M defined by $\boldsymbol{x}_{0,i} = \psi(\theta_i)$ with $\theta_i = 2\,\pi\,(i-1)/N$, $i = 1, \ldots, N$. Figure 10 shows how the points $\boldsymbol{x}_{0,i}$ look like in different coordinate spaces, illustrating that the $\dot{x}$–$\dot{y}$ coordinate plane could be used to effectively parametrize the intersection between the quasi-periodic torus and the surface of section $S(\boldsymbol{x}) = z$, $\dot{z} < 0$. To that end, let $R = \sqrt{\dot{x}^2 + \dot{y}^2}$, and consider a truncated Fourier series up to the $N_{max} = 20$ order such that

$$\boldsymbol{X}_0 = \begin{bmatrix} \boldsymbol{x}_{0,1} \\ \vdots \\ \boldsymbol{x}_{0,N} \end{bmatrix} = A(\theta)\, \boldsymbol{Q}, \tag{34}$$

where $\boldsymbol{Q} = \begin{bmatrix} \boldsymbol{Q}_x^T & \boldsymbol{Q}_y^T & \boldsymbol{Q}_R^T & \boldsymbol{Q}_{\dot{z}}^T \end{bmatrix}^T$ is the $(8\,N_{\text{max}} + 4) \times 1$ Fourier coefficient vector (since $z = 0$ on the surface of section, there is no need to compute the corresponding Fourier coefficient vector) and $A(\theta)$ is the $6\,N \times (8\,N_{\text{max}} + 4)$ matrix defined by

$$A(\theta) = \begin{bmatrix} A(\theta_1) \\ \vdots \\ A(\theta_N) \end{bmatrix}, \qquad A(\theta_i) = \begin{bmatrix} \text{cs}(\theta_i) & 0 & 0 & 0 \\ 0 & \text{cs}(\theta_i) & 0 & 0 \\ 0 & 0 & 0 & 0 \\ 0 & 0 & \cos(\theta_i)\,\text{cs}(\theta_i) & 0 \\ 0 & 0 & \sin(\theta_i)\,\text{cs}(\theta_i) & 0 \\ 0 & 0 & 0 & \text{cs}(\theta_i) \end{bmatrix} \tag{35}$$

with

$$\text{cs}(\theta_i) = \begin{bmatrix} 1 & \cos(\theta_i) & \sin(\theta_i) & \cos(2\,\theta_i) & \sin(2\,\theta_i) & \dots & \cos(N_{\text{max}}\,\theta_i) & \sin(N_{\text{max}}\,\theta_i) \end{bmatrix}. \tag{36}$$

Now propagate each of the N points till the next surface of section crossing using the full nonlinear equations of motion (15), and compute the corresponding angle in terms of the chosen coordinate variable, i.e.,

$$\theta_{T,i} = \arctan\left(\frac{\dot{y}_i}{\dot{x}_i}\right). \tag{37}$$

If the $\boldsymbol{X}_0$ points were initialized exactly on the invariant set of the Poincaré section, the points obtained after one orbital period, namely $\boldsymbol{X}_T$, would satisfy

$$F(\boldsymbol{Q}) = \boldsymbol{X}_T - A(\theta_T)\,\boldsymbol{Q} = \boldsymbol{0}. \tag{38}$$

Since this is not the case–at least for the very first initial guess–consider updating the Fourier coefficients using the Newton's iteration scheme

$$\boldsymbol{Q}^{k+1} = \boldsymbol{Q}^k - DF(\boldsymbol{Q}^k)^\dagger\, F(\boldsymbol{Q}^k), \tag{39}$$

where $DF^\dagger$ denotes the pseudoinverse of the jacobian matrix of $F(\boldsymbol{Q})$ (see Koleman's original paper for details on how to compute the Jacobian matrix).

Before that, observe that quasi-periodic orbits are 2D objects in a six-dimensional phase space. Therefore, two properties need to be specified in order to define a quasi-periodic orbit uniquely. It turns out that the best choice of parameters to achieve bounded relative motion is made by the area of the invariant set in the $\dot{x}$–$\dot{y}$ plane, namely

$$\mathcal{A} = \frac{\pi}{2}\,\boldsymbol{Q}_R^T\,\boldsymbol{Q}_R, \tag{40}$$

and the period of the quasi-periodic orbit, i.e.,

$$T = \frac{1}{N}\sum_{i=1}^{N} \tau(\boldsymbol{x}_i), \tag{41}$$

where $\tau(\boldsymbol{x}_i)$ is the time between two consecutive surface of section crossings for the i-th trajectory. Thus, consider augmenting the error vector $F(\boldsymbol{Q})$ with

$$F(\boldsymbol{Q}) = [\boldsymbol{X}_T - A(\theta_T)\,\boldsymbol{Q};\ \Delta\mathcal{A};\ \Delta T], \tag{42}$$

where $\Delta\mathcal{A} = \mathcal{A} - \mathcal{A}_{\text{desired}}$ and $\Delta T = T - T_{\text{desired}}$ are the differences between the current and desired values. Then, the algorithm usually converges to the desired quasi-periodic orbit in four or five iterations.

FORMATION FLYING

By choosing $\lambda = \lambda_{12}$, $\kappa = 50$ m, $\mathcal{A}_{\text{desired}}$ equal to the $\dot{x}$–$\dot{y}$ area of Figure 10, and T_{desired} equal to the period of the periodic orbit of Figure 7b, the algorithm converges after four iterations to a quasi-periodic torus that yields the relative motion of Figures 11. In the plots of Figure 11, the chief spacecraft has been initialized on the periodic orbit, whereas the deputy spacecraft has been initialized on one of the quasi-periodic orbits obtained with the Newton iteration scheme. The resulting **in-plane** relative trajectories of the satellites are integrated using the equations of motion (15) for 30 days.

Although there is some residual drift in the along-track direction, the relative trajectory computed with quasi-periodic initial conditions does not diverge as fast as the relative trajectory computed from the linear approximation of the invariant torus (i.e., using as initial conditions one of the $\boldsymbol{x}_{0,i}$ points created on the invariant set of the monodromy map M). Similar results are also obtained when initializing the deputy spacecraft on the quasi-periodic torus computed for the second center manifold, i.e., $\lambda = \lambda_{34}$, $\boldsymbol{v} = \boldsymbol{v}_{34} = \boldsymbol{v}_3 + \mathrm{i}\,\boldsymbol{v}_4$. The obtained **out-of-plane** relative trajetories are illustrated in Figure 12.

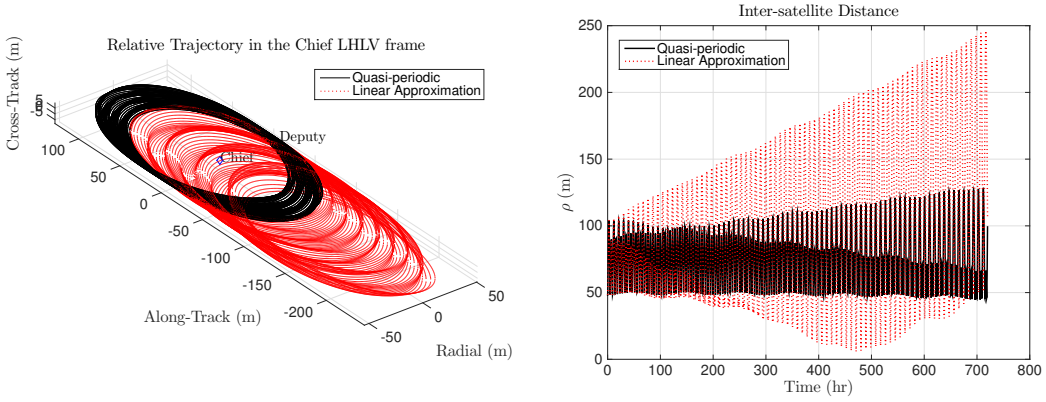

Figure 11: In-plane Relative Trajectories over 30 days. The chief spacecraft has been initialized on the periodic orbit.

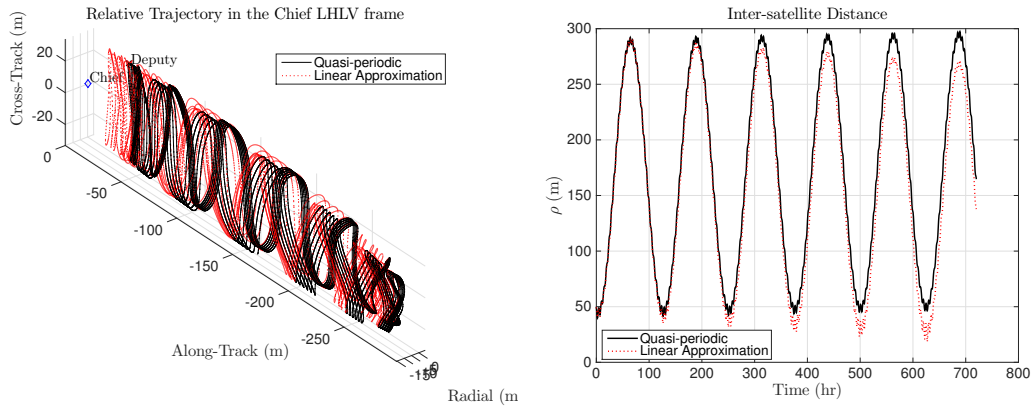

Figure 12: Out-of-plane Relative Trajectories over 30 days. The chief spacecraft has been initialized on the periodic orbit.

Another interesting design option would be to initialize both the chief and the deputy satellites on the invariant torus. Figures 13 and 14 display how the relative trajectory looks like for spacecraft formations on the first and second center manifold respectively. As it can be seen, bounded relative motion about slowly rotating tri-axial ellipsoids can be achieved over long time spans; i.e., more than 30 days.

It is important to note that these results are obtained using the full constant density ellipsoidal gravity model of the central body. However, the plots of Figures 10 and 14 also assume perfect initial conditions and do not take into account the effects of other forces such as solar radiation pressure and third body attraction. As one can expect, including these perturbations in the simulations leads to unstable relative motion, which would eventually require active control strategies to mitigate the relative drift induced by

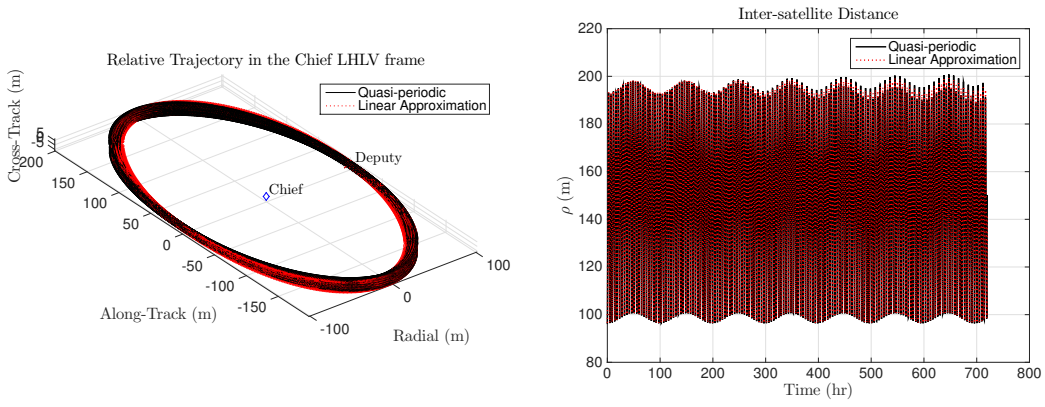

Figure 13: In-plane Relative Trajectory over 30 days. Satellites are both initialized on the invariant torus.

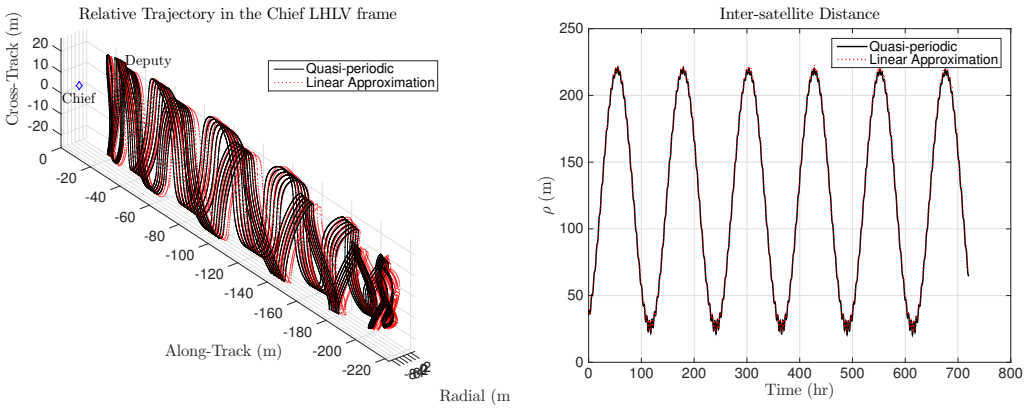

Figure 14: Quasi-pendulum Relative Trajectories over 30 days. Satellites are both initialized on the invariant torus.

the errors in the system. Yet, even in a worst case scenario where the deputy and chief spacecraft are deployed when Toutatis is at perihelion, control wouldn't be necessary for more than 2.5 days (Figure 15). In this time frame, many scientific operations could be performed and used to infer valuable information on the mechanical and chemical properties of the target asteroid.

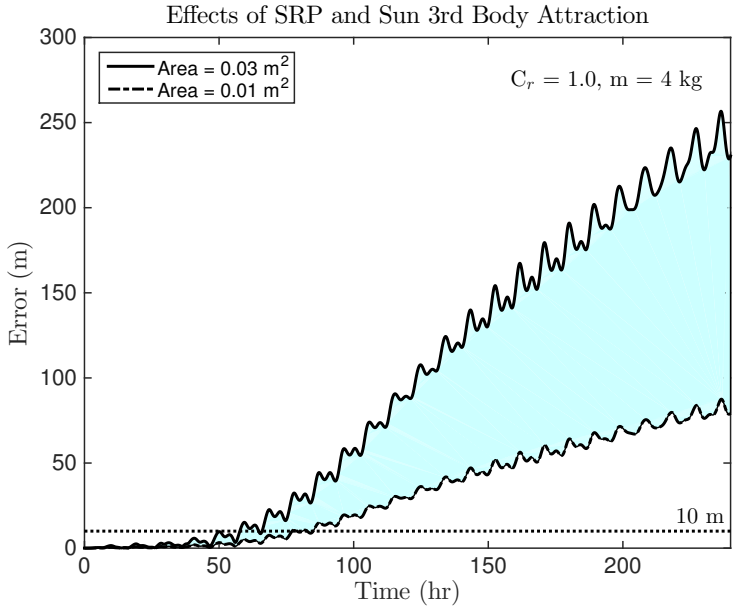

Figure 15: Effects of SRP and Sun Third body attraction on 3U Cubesat Formations about Toutatis at Perihelion.

CONCLUSIONS AND FUTURE WORK

By combining analytical and numerical methods, it is possible to come up with a systematic procedure to initialize spacecraft formations about 4179 Toutatis. The problem was first analyzed with a second-order second-degree gravity field, which was initially used to derive first-order differential relationships between the mean orbit elements of the spacecraft. The second-order second-degree bounded relative motion conditions derived in this paper were seeking to minimize the relative drift between the satellite in the formations caused by the elongated shape of the central body. However, this method fails to provide long-term bounded relative orbits because of the approximations and errors in the Lie-Deprit transformation used to carry on the necessary mean-to-osculating orbit element conversions.

Such mapping, however, turns out to be necessary to provide a reliable initial guess for the numerical computation of periodic orbits in the body-fixed frame of the asteroid (Figure 7). Since the monodromy matrix computed along these trajectories has two pairs of complex conjugate eigenvalues, the computed periodic orbits are stable and surrounded by two center manifolds. Because of this, Koleman's surface of section approach was applied to extend these manifolds beyond the linear regime, and used to compute families of quasi-periodic orbits about Toutatis.[2] In particular, by choosing the orbital period as one of the parameters in Koleman's method, it was possible to come up with invariant tori foliated by quasi-periodic orbits of the same period. This is an ideal condition for bounded relative motion as it yields in-plane and out-of-plane relative trajectories that remain bounded for more than 30 days (Figures 13 and 14).

Future work will be focused on extending this approach beyond slowly rotating bodies and applying dynamical systems theory to design spacecraft formations about planets and general asteroids. Furthermore, it will be interesting to investigate the existence of cost-free bounded relative trajectories with more sophisticated gravity fields such as the constant density polyhedron model, which better takes into account the actual physical shape of the target asteroid.[15] Finally, solar radiation pressure should be modeled and included in the equations of motion to improve robustness.

REFERENCES

[1] W. Hu and D. J. Scheeres, "Spacecraft motion about slowly rotating asteroids," *Journal of guidance, control, and dynamics*, vol. 25, no. 4, pp. 765–775, 2002.

[2] E. Kolemen, N. J. Kasdin, and P. Gurfil, "Multiple poincaré sections method for finding the quasiperiodic orbits of the restricted three body problem," *Celestial Mechanics and Dynamical Astronomy*, vol. 112, no. 1, pp. 47–74, 2012.

[3] C. Maddock, J. P. Sanchez Cuartielles, M. Vasile, and G. Radice, "Comparison of single and multi-spacecraft configurations for nea deflection by solar sublimation,"

in *New Trends in Astrodynamics and Applications III(AIP Conference Proceedings Volume 886)*, vol. 886, pp. 303–316, 2007.

[4] S. Gong, J. Li, and H. BaoYin, "Formation flying solar-sail gravity tractors in displaced orbit for towing near-earth asteroids," *Celestial Mechanics and Dynamical Astronomy*, vol. 105, no. 1-3, pp. 159–177, 2009.

[5] M. Vasile and C. A. Maddock, "On the deflection of asteroids with mirrors," *Celestial Mechanics and Dynamical Astronomy*, vol. 107, no. 1-2, pp. 265–284, 2010.

[6] C. Foster, J. Bellerose, D. Mauro, and B. Jaroux, "Mission concepts and operations for asteroid mitigation involving multiple gravity tractors," *Acta Astronautica*, vol. 90, no. 1, pp. 112–118, 2013.

[7] J. Huang, J. Ji, P. Ye, X. Wang, J. Yan, L. Meng, S. Wang, C. Li, Y. Li, D. Qiao, *et al.*, "The ginger-shaped asteroid 4179 toutatis: New observations from a successful flyby of chang'e-2," *Scientific reports*, vol. 3, 2013.

[8] H. Schaub and K. T. Alfriend, "J2-invariant relative orbits for spacecraft formations," *Celestial Mechanics and Dynamical Astronomy*, vol. 79, no. 2, pp. 77–95, 2001.

[9] D. J. Scheeres, *Orbital Motion in Strongly Perturbed Environments*. Springer, 2012.

[10] H. Schaub and J. L. Junkins, *Analytical Mechanics of Space Systems*. AIAA Education Series, 2nd ed., 2009.

[11] A. Deprit, "Canonical transformations depending on a small parameter," *Celestial Mechanics*, vol. 1, no. 1, pp. 12–30, 1969.

[12] B. De Saedeleer and J. Henrard, "The combined effect of j2 and c22 on the critical inclination of a lunar orbiter," *Advances in Space Research*, vol. 37, no. 1, pp. 80–87, 2006.

[13] R. S. Hudson and S. J. Ostro, "Shape and non-principal axis spin state of asteroid 4179 toutatis," *Science*, pp. 84–84, 1995.

[14] D. J. Scheeres, "Dynamics about uniformly rotating triaxial ellipsoids: Applications to asteroids," *Icarus*, vol. 110, no. 2, pp. 225–238, 1994.

[15] R. A. Werner and D. J. Scheeres, "Exterior gravitation of a polyhedron derived and compared with harmonic and mascon gravitation representations of asteroid 4769 castalia," *Celestial Mechanics and Dynamical Astronomy*, vol. 65, no. 3, pp. 313–344, 1996.